Depósito de investigación de la Universidad de Sevilla

https://idus.us.es/

Esta es la versión aceptada del artículo publicado en:

This is an accepted manuscript of a paper published in:

ACS Chemical Neuroscience: 2019

DOI: 10.1021/acschemneuro.9b00088.

Copyright: © 2019 American Chemical Society

El acceso a la versión publicada del artículo puede requerir la suscripción de la revista.

Access to the published version may require subscription.

"This article has been published in a revised form in [ACS Chemical Neuroscience] [10.1021/acschemneuro.9b00088.]. This version is free to download for private research and study only. Not for redistribution, re-sale or use in derivative Works".

Differential interactome and innate immune response activation of two structurally distinct misfolded protein oligomers.

Benedetta Mannini[1], Giulia Vecchi[1], Adahir Labrador-Garrido[2,3], Bertrand Fabre[4], Kathryn Lilley[4], David Pozo[2,3*], Michele Vendruscolo[1], Fabrizio Chiti[5], Christopher M. Dobson[1*], Cintia Roodveldt[2,3*]

[1]Centre for Misfolding Diseases, Department of Chemistry, University of Cambridge, Cambridge, UK
[2]Andalusian Center for Molecular Biology and Regenerative Medicine (CABIMER), Universidad de Sevilla-Consejo Superior de Investigaciones Científicas (CSIC) Universidad Pablo de Olavide, Seville, Spain
[3]Department of Medical Biochemistry, Molecular Biology and Immunology, Universidad de Sevilla, Seville, Spain
[4]Cambridge Centre for Proteomics, Systems Biology Centre, Department of Biochemistry, University of Cambridge, Cambridge, UK
[5]Department of Biomedical Experimental and Clinical Sciences, Section of Biochemistry, University of Florence, Florence, Italy

ABSTRACT: The formation of misfolded protein oligomers during early stages of amyloid aggregation and the activation of the inflammatory response are two characteristic events associated with the onset and progression of a wide range of neurodegenerative diseases. Although it has been established that misfolded oligomers are involved in the neuroinflammatory process, the links between their structural and physicochemical features and their functional effects on the immune response remain largely unknown. To explore such links, we have taken advantage of two structurally distinct and well-characterized types of soluble oligomers of the protein HypF-N, denoted type A and B, which have been shown to have different surface-exposed hydrophobicity and cytotoxicity. We analysed the microglial inflammatory response triggered by these oligomers and found that, even though they both stimulate the release of pro-inflammatory cytokines, type B oligomers induced a substantially greater response than type A oligomers. By using a combination of confocal microscopy, protein pull-down assays and high-throughput mass spectrometric-based proteomic analysis, we found that the two types of oligomers interact differentially with microglial cells. In particular, despite the fact that both types of oligomers were found to bind to a common pool of microglial proteins, type B relative to type A oligomers showed enhanced protein binding, a finding that correlated with the observed inflammatory response. In addition, the receptors and signalling molecules in the interactome associated with inflammatory-mediated neurodegeneration revealed a number of previously unidentified proteins likely to be involved in the oligomer-elicited innate immune response.

INTRODUCTION

The misfolding and aggregation of proteins into amyloid fibrils is the hallmark of a wide range of human neurodegenerative disorders, including Alzheimer's disease (AD), Parkinson's disease (PD), Hungtington's disease (HD) and amyotrophic lateral sclerosis (ALS) [1]. Increasing evidence suggests that the soluble oligomeric species preceding fibril formation, or released by mature fibrils, are believed to be responsible for generating cellular dysfunction through a variety of mechanisms [2 3 4 5 6 7 8]. Thus, a comprehensive understanding of such mechanisms is vital for designing effective approaches for diagnostic and therapeutic interventions [9 10 11].

The chronic neuroinflammatory state resulting from the massive microglial activation that develops in neurodegenerative diseases including PD [12], AD [13], HD [14] and ALS (Roodveldt et al., Trends Mol. Med. in press), is known to be a central feature in the development of these pathologies [15]. It has become established that neurodegeneration can progress in a non-neuronal autonomous manner in which glial cells actively contribute to neuronal death by generating and sustaining neuroinflammation [16 15].

Oligomers formed during the aggregation of a series of different proteins have generally been found to share a range of physicochemical characteristics, including a significant content of β-sheet structure, a small size (compared to amyloid fibrils), a high exposure of hydrophobic surfaces to the solvent and a strong reactivity to conformation-specific antibodies [17]. Such physicochemical properties have also been found to be determinants of the cellular toxicity of the oligomers [18 19 20 2 21 22]. However, the impact of the physicochemical features of such oligomers on microglial responses in the context of misfolding diseases is still unknown. In this context, it has been suggested that the main trigger of innate immunity is the aberrant exposure of hydrophobic surfaces in certain biological molecules and assemblies [23 24], and such exposed regions are likely to be characteristic of virtually all misfolded protein aggregates [25 19 2 21 22]. It remains to be established, however, how the structural, physicochemical and biological features of these potentially pathogenic species are correlated with the stimulation of an innate immune response.

The aggregates formed by misfolded and amyloidogenic proteins have been recognized as potential triggers of inflammation in the context of neurodegenerative disorders [14 16]. A number of disease-linked protein oligomers present in the extracellular medium have been shown to elicit strong inflammatory responses in microglia, which are the principal

immunocompetent cells in the central nervous system (CNS), by acting as potent danger-associated molecular patterns (DAMPs) and strongly activating innate immunity [26 27 28 29].

In the present study we investigated the inflammatory response triggered by misfolded oligomers of the N-terminal domain of the HypF protein from E. coli (HypF-N). This protein is a convenient model system for exploring the link between neurodegeneration and protein aggregation for a number of reasons. First, under conditions that destabilize its native structure it forms oligomers and amyloid fibrils in vitro that are closely similar to those observed for proteins associated with human diseases [2 30 31 32 33]. Second, HypF-N oligomers formed in vitro impair cellular viability in a similar manner to protein oligomers associated with many amyloid diseases, both when added to the extracellular medium of cultured cells [34 35 36 37 38 21 39] and when administered directly into the brain in experiments with animal models [40 39]. Third, HypF-N oligomers co-localise with protein dense regions in the postsynaptic membrane of cultured neurons, inhibit long-term potentiation in hippocampal slices and induce cognitive impairment upon administration into rat brains, all of which are recognised biochemical, electrophysiological and biological effects of the Aβ42 oligomers associated with AD [41]. Fourth, HypF-N oligomers are stable and maintain their morphological and structural properties under a wide range of experimental conditions, allowing detailed structural, biological and functional studies to be carried out [2 37 21 41 39]. Finally, and of particular importance in the context of the present study, the nature and cytotoxicity of the different types of HypF-N oligomers is clearly different: indeed, those designated as type A are cytotoxic toward neuroblastoma cells and primary neurons, and in animal models, while type B do not elicit such effects [2 39].

Despite their different cytotoxic properties, these two types of oligomers share a similar size and morphology when observed by atomic force microscopy [2]. In fact, both oligomer types are roughly spherical, with diameters of 2-6 nm, and have similar thioflavin T (ThT) binding properties that are indicative of prefibrillar, amyloidogenic structures [2]. Characterization of these species at a molecular level, however, revealed that the toxic type A oligomers have a higher degree of surface hydrophobicity than the benign type B oligomers, indicating a potential causative link between such structural characteristics and cytotoxicity [2 21 22].

In the present study, by examining the effects of the these well-characterized and robust HypF-N oligomers on microglial cells, we report that the hydrophobicity and degree of interaction of the oligomers with the microglial proteome are highly correlated with the elicited immune response. Moreover, we identify the immune interactome for both oligomer types, which enables the identification of key proteins responsible for aggregate-elicited microglial neuroinflammation.

RESULTS

Low concentrations of oligomers do not affect cell viability but trigger inflammation. We first tested the ability of type A and type B oligomers to stimulate N13 microglial cells in culture. For this purpose, we searched for conditions in which neither type of oligomers affected cellular viability, so that we could enable a direct comparison of the inflammatory responses triggered by the two types of aggregates. We carried out a MTT reduction test, a standard assay based on mitochondrial metabolic integrity as a readout of cell viability, on N13 cells treated for 24 h with different concentrations of type A or type B HypF-N oligomers (Figure 1). As previously shown with a variety of cell lines, including human neuroblastoma (SH-SY5Y), mouse endothelial (Hend), Chinese hamster ovary (CHO), and human embryonic kidney 293 (HEK293) cells [2 21 38 42 43], at a concentration of 12 μM (monomer equivalents), the two types of oligomers showed a marked difference in cytotoxicity, with type A aggregates causing a 30% decrease in cell viability and type B oligomers appearing essentially innocuous (Figure 1). In N13 cells the cytotoxic effect of type A oligomers decreased in a dose-dependent manner and at concentrations below 4.3 μM did not detectably alter cell viability, whereas type B oligomers were found to be innocuous at all concentrations tested (Figure 1).

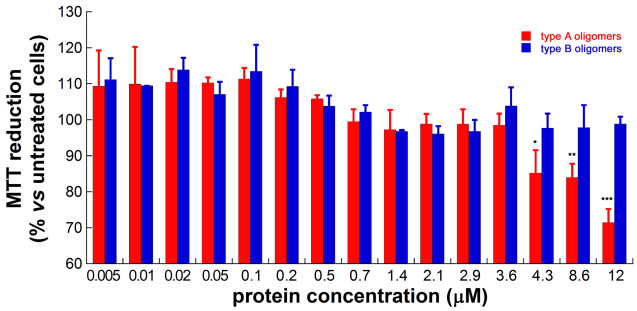

Figure 1. Viability of N13 microglia cells after treatment with type A and type B oligomers. **The degree of MTT reduction for murine N13 microglial cells treated for 24 h with different concentrations (in monomer equivalents) of type A (red) and type B (blue) oligomers added to the extracellular medium. The error bars correspond to standard errors of the means (SEM) of four independent experiments (n=4). Single, double, and triple asterisks (*) refer to p<0.05, p<0.01, and p<0.001, respectively, with respect to untreated cells.**

We next determined by ELISA assays the levels of a set of key disease-linked immune mediators, namely the pro-inflammatory IL-1β, IL-6, and TNFα cytokines, and the anti-inflammatory IL-10 cytokine, after incubation of N13 cells with type A or B oligomers for 6 h or 24 h (Figure 2). As a positive control, we used bacterial lipopolysaccharide (LPS) as a conventional stimulus to assess the innate immune response by N13 cells where all four cytokines tested have been shown to be increased upon LPS engagement [44]. Compared to untreated cells, the release of IL-1β elicited by the type B oligomers was found to be significantly higher at all concentrations tested, the lowest being 0.005 μM (monomer equivalents), whereas in the case of type A aggregates it was significantly higher only when present at the highest concentrations tested in this study, above 8.6 μM (monomer equivalents). Both types of oligomers induced the release of IL-6 at concentrations above 0.05 μM and 0.02 μM (monomer equivalents), for type A and B, respectively. The amount of TNFα detected for cells treated with type A and type B oligomers was significantly higher than that for untreated cells, with effects still detectable at concentrations of 0.1 μM and of 0.005 μM (monomer equivalents), respectively. Stimulation of cells with native non-aggregated HypF-N protein at 0.125 μM, 0.25 μM, 2 μM and 8 μM resulted in the secretion of two cytokines tested in this study, IL-6 and TNFα at levels indistinguishable from untreated cells (Supplementary Figure 1).

We found, in addition, that treatment with either type of oligomer at concentrations below 12 μM did not stimulate the release of the anti-inflammatory cytokine IL-10; indeed, the levels of IL-10 detected in the presence of both type A and B

oligomers were lower than those found in the untreated cells (Figure 2). Only at oligomer concentrations of 12 μM (monomer equivalents), the highest tested here, were the IL-10 levels significantly higher than those of untreated cells.

Three conclusions can be drawn from these data. First, the levels of the released pro-inflammatory mediators IL-1β, IL-6 and TNFα, and the lack of stimulation of IL-10 secretion, except at very high concentrations, indicate that both types of oligomers elicit a significant pro-inflammatory response but not an immunoregulatory one. Second, the concentration of HypF-N oligomers able to trigger an inflammatory response is about three orders of magnitude lower than that needed to cause cytotoxicity, suggesting that the inflammatory response could be particularly important during the early events of the protein aggregation process, when the concentration of misfolded protein oligomers is still very low. Third, the two types of oligomers have a different ability to induce the release of cytokines, as we will discuss in detail below.

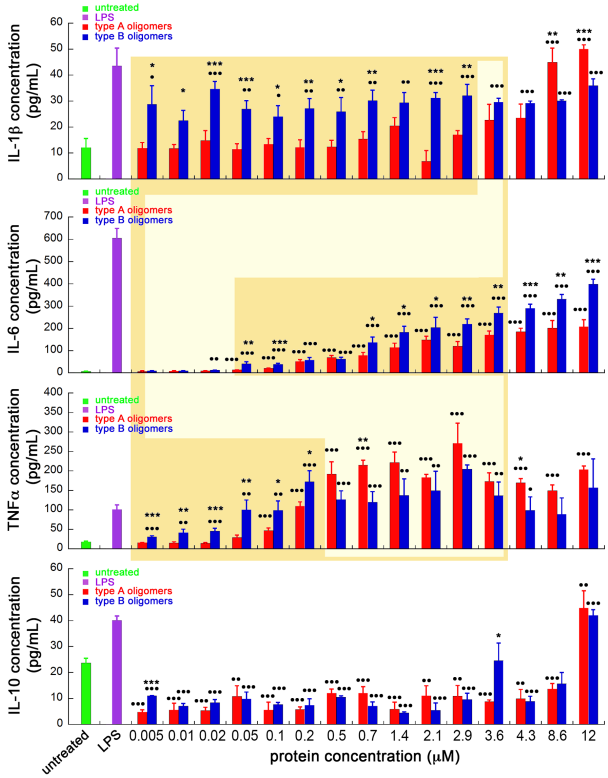

Figure 2. Cytokine release profile of N13 microglia cells after treatment with type A and type B oligomers. **The release of IL-1β, IL-6, TNFα and IL-10 was measured by ELISA assays in the supernatants of cultured N13 cells treated with different concentrations of type A and type B oligomers (in monomer equivalents). The culture medium with and without addition of lipopolysaccharide (LPS) was used as a negative and positive control, respectively. The error bars correspond to standard errors of the mean (SEM) of 4 independent experiments (n=4). The shaded area in yellow indicates the range between 0.005 and 3.6 μM, where the oligomers are unable to cause cell death as assessed by the MTT reduction viability test. Single, double, and triple asterisks (*) refer to p<0.05, p<0.01, and p<0.001, respectively, with respect to cells treated with the other type of oligomers at the same concentration. Single, double, and triple points (•) refer to p<0.05, p<0.01, and p<0.001, respectively, relative to untreated cells.**

The two types of oligomers display different abilities to elicit a pro-inflammatory response. The comparison between the release of cytokines mediated by the two types of oligomers showed that type B are more potent than type A in triggering the release at low concentrations of all three pro-inflammatory mediators tested. The levels of IL-1β and TNFα were significantly higher when microglia cells were treated with type B than with type A oligomers, from a concentration of 0.005 μM, the lowest tested here, up to 2.9 μM and 0.2 μM, respectively; the release of IL-6 was significantly higher for type B oligomers at almost all the concentrations where an effect was observed, i.e. at concentrations above 0.05 μM. For clarity, the ranges in which type B oligomers were found to be more efficient respect to type A oligomers have been highlighted in Figure 2 with a dark yellow shaded area. At the protein concentrations in which the viability of cells was observed to be affected by the type A oligomers, the levels of the two cytokines, IL-1β and TNFα, are similar for both types of oligomers, although at the highest protein concentrations, type A oligomers were more potent. In conclusion, these sets of data show that at low concentrations of oligomers, at which the cell viability is not detectably compromised (light yellow shaded area in Figure 2), type B oligomers are stronger inducers of the inflammatory response than type A oligomers.

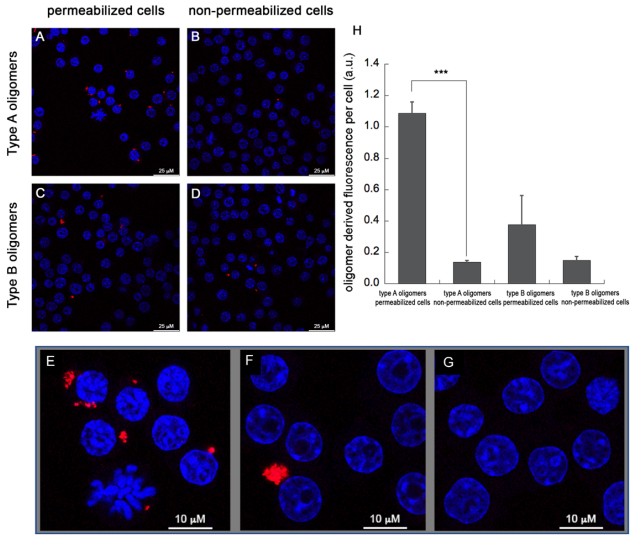

Figure 3. Interaction of type A and B oligomers with the surfaces of N13 cells. **(A-G) Representative confocal microscopy images showing the interaction of the oligomers with the cultured N13 cells. Cells were incubated for 24 h with type A (A, B) or B (C, D) oligomers and then washed. The samples were then permeabilized by using 0.5% (v/v) Triton X-100 (A, C) or not permeabilized (B, D). The red fluorescence arises from the immunolabelling of the oligomers and the blue indicates the nuclei stained with DAPI. In (E) and (F) enlarged images from (A) and (C), respectively, are shown. (G) Untreated cells. (H) Quantification of the fluorescence emission arising from the oligomers normalized to the number of cells labelled with Alexa Fluor 633-conjugated secondary antibodies. The error bars correspond to standard deviations of the mean of three different fields. Triple asterisks refer to p<0.001 relative to permeabilized cells.**

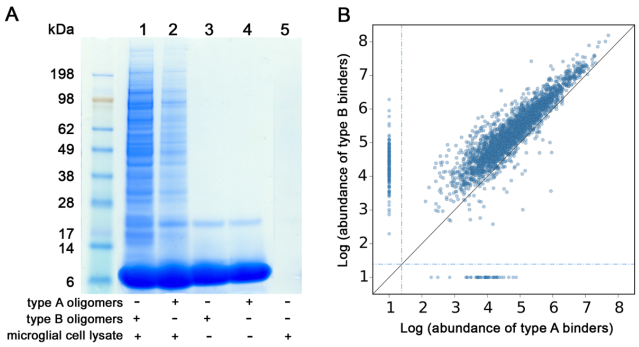

Figure 4. Interaction of type A and B oligomers with the protein components of N13 cells. **(A) Pull-down assay using type A and type B oligomers incubated for 1 h in isolation or in combination with microglial N13 cell lysates. (B) Log10 abundances (iBAQ values) of proteins binding to type B oligomers compared to type A oligomers as obtained by proteomic analysis. Each blue point is a protein detected and quantified. Points within the dashed line have been detected in pull-downs with only one of the two oligomers, and have been assigned with a default value of 1 in order to allow their graphical representation. The points on the left side of the plot are proteins detected to bind only to the type B oligomers, while points on the lower edge of the plot are proteins detected to bind only to the type A oligomers.**

Type A and B oligomers exhibit differential penetration profiles across the cell membrane. To shed light on the molecular mechanisms responsible for the differential immunogenic activity of the oligomers, we investigated their ability to interact with cell surfaces and their propensity to become internalized within cells. First, we evaluated the ability of the oligomers to penetrate the membranes of N13 cells by means of immunofluorescence (IF) and confocal microscopy analysis (Figure 3A-G). Cultured cells were incubated in the presence of either 0.7 μM (monomer equivalents) of type A or type B oligomers added to the extracellular medium for 24 h, washed thoroughly, and then either permeabilized or left non-permeabilized before labelling with anti-HypF-N primary antibodies and subsequently with Alexa Fluor 633-conjugated secondary antibodies (red fluorescence). Cell nuclei were stained with 4',6-diamidino-2-phenylindole (DAPI, blue fluorescence). In non-permeabilized cells, the antibodies are unable to enter the cells and hence cannot detect any oligomers located inside them; any red fluorescence signal must therefore arise from HypF-N aggregates outside the cells or attached to cell membranes. By contrast, in the permeabilized samples the antibody can penetrate the membrane and the red fluorescence can result from the oligomers inside or outside the cells [45].

Numerous red fluorescent puncta are visible within the permeabilized cells treated with type A oligomers (Figure 3A and at higher magnification in Figure 3E), whereas such puncta are hardly detectable in the non-permeabilized cells (Figure 3B). These results suggest that the majority of the type A oligomers added to the cell media were localized within the cells. In the images obtained from cells incubated with type B oligomers, the numbers of red puncta visible in the permeabilized cells (Figure 3C and magnification in Figure 3F) and non-permeabilized cells (Figure 3D) are similar, indicating that the number of oligomers that had penetrated the cell membrane was very low and that the majority of oligomers were attached to the cell surfaces. These data are summarized in Figure 3H showing the quantification of the fluorescence signals derived from the oligomers.

Type A and B oligomers bind to a common pool of membrane proteins in microglial cells but with different affinities. As a second part of this study, we assessed the ability of the two different types of oligomers to bind to the proteins present within N13 cells. To this aim, we performed pull-down experiments by incubating type A and type B oligomers for 1 h in isolation or in combination with proteins extracted from N13 cell lysates. During the protein extraction step, the membrane protein fraction that would otherwise be under-represented was enriched by using an appropriate protein lysis protocol to ensure that these proteins remained in their native conformations despite the absence of the lipid membrane (see Methods section for details). After incubation with the extracts, the oligomers were pulled down by centrifugation and the pelleted fractions were analyzed by SDS-PAGE (Figure 4A). The results indicate that type B oligomers have a generally higher ability than type A oligomers to bind to proteins, indicating a higher preference of type B oligomers for the protein component of the membrane. As a control, no proteins from N13 cells were found in the pellet fraction in lysates incubated in the absence of either type of oligomer (Figure 4A).

We then subjected the protein fractions pulled-down with type A and type B oligomers to liquid chromatography-tandem mass spectrometry (GeLC-MS/MS) followed by high-throughput proteomic analysis in order to assess and compare the N13 cell interactome of the two oligomers, i.e. the set of proteins bound in each case. The result of a representative experiment is shown in Figure 4B and indicates the abundance of the proteins bound to type B oligomers compared to type A oligomers. Analysis of the data supports the conclusion from the pull-down experiments, as the large majority (>90%) of the common binders are above the bisector line (Figure 4B), indicating a higher protein binding capability of type B compared to type A oligomers. It is also evident that only a small number of proteins have a single value of abundance (Figure 4B, horizontal and vertical points within the dashed blue lines), indicating that they were detected to bind to only one type of oligomer in that replica.

In order to identify the proteins that could be key players in the microglial immune response to the oligomers, we selected for additional analyses only those proteins known to be located on cell membranes, by filtering the N13 cell interactomes of both types of oligomers on the basis of their subcellular locations reported in the UniProt database [46]. Figure 5A shows the abundances of N13 membrane proteins found in the pull-down samples of type B compared to type A oligomers. Proteins detected to bind to only one type of oligomer (type A or type B) in a given replica are reported on the left and lower edge of each graph, within the dashed blue lines (horizontal or vertical points, respectively). The data reveal that the results for the membrane proteins alone are very similar to those obtained for all proteins (Figure 4B), as the majority of the shared points (Figure 5A) (>95% in total) are again above the bisector line. The results, therefore, reveal that type B oligomers have a higher ability than type A oligomers to bind to the set of membrane proteins of microglial cells (Figure 5A). They also show that type B oligomers have a higher ability than type A oligomers to bind to native cytosolic proteins, indicating that they have a higher general propensity to bind to both types of proteins (Supplementary Figure 2).

To shed light on the identity of the membrane proteins of N13 cells present in the interactomes obtained for the two types of oligomer, we combined the results of all the independent pull-down GeLC-MS/MS experiments (biological replicas) in each case. We then defined as 'common binders' those proteins detected in at least two biological replicas for each oligomer type, and as 'specific binders' those proteins detected at least twice for a single type of oligomer, but never for the other type. We found that 518 membrane proteins out of 573 (90.4% of all the membrane proteins detected in this study) are common binders of both types of oligomer and that the relative proportion of each protein is essentially the same in the pull-down assays for the two types of oligomer (Figure 5B). These results show, therefore, that the large majority of the membrane proteins interact with both types of oligomer (i.e. are common binders) and their relative abundances are independent of the type of oligomer to which they bind. Only a very small number of proteins (14) are found to be specific binders; of these, 12 are for type B oligomers (~2.1%) and 2 are for type A oligomers (~0.3%) (Figure 5B, left and bottom shaded area respectively). Nevertheless, even though type A and B oligomers bind to essentially the same pool of proteins (Figure 4B), albeit with significantly different affinities (Figure 5A), there are 14 proteins that appear to be specific binders.

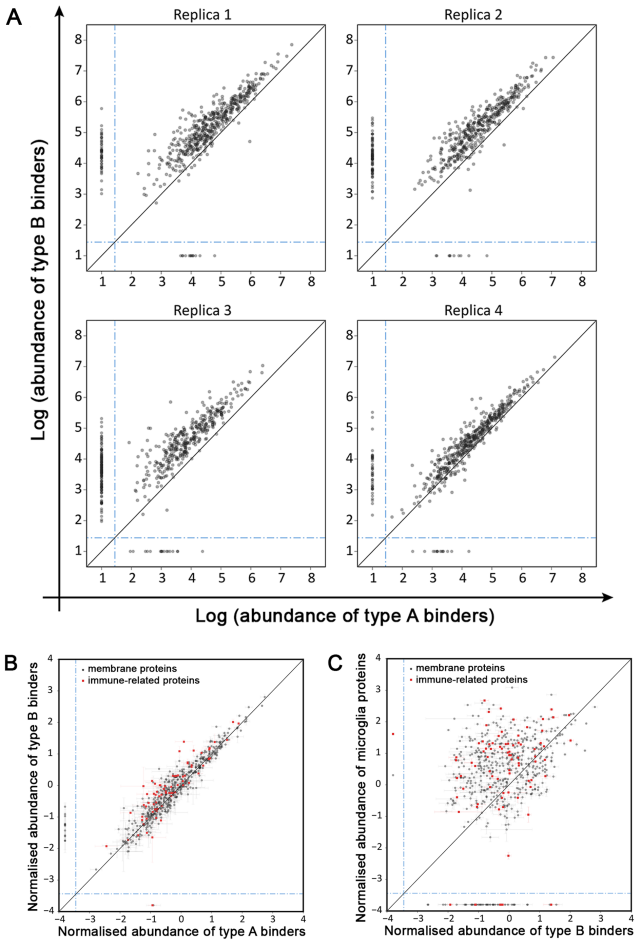

Figure 5. Interaction of type A and B oligomers with membrane proteins from N13 cells. **(A) Replica-specific scatterplot of protein abundances (log10 iBAQ values) of N13 microglia cell membrane proteins bound to type B oligomers (y axis) vs those bound to type A oligomers (x axis) from the four biological replicas analysed in this study. The black points in each subplot represent membrane proteins detected and quantified in each replica. Proteins shown vertically on the left side and horizontally on the lower edge of each scatterplot within the dashed blue lines are membrane proteins binding to type B and type A oligomers, respectively. (B-C) Scatterplot of the normalised protein abundances comparing type A and type B oligomers. The abundance of each membrane protein detected in at least two replicas has been averaged and normalised over the biological replicas (see Materials and Methods). The points shown vertically and horizontally within the dashed blue lines in the left side and lower edge of the plot are proteins detected to interact with one type of oligomer but not the other. The red square points are membrane proteins known to be associated with the immune response. The errors are median absolute deviations corrected with the propagation law of errors for the z-score normalisation. (B) Scatterplot of the normalised abundances of membrane proteins binding to type B vs type A oligomers. Proteins on the left side of the plot within the dashed blue lines are type B 'specific binders', while proteins on the lower edge are type A 'specific binders.' (C) Scatterplot of the normalised abundances of the total set of membrane proteins in microglia, obtained from available MS data [47] *vs* those found to bind to type B oligomers.**

The interactome of HypF-N oligomers suggests key proteins in microglia immune signaling. Of the 518 membrane proteins found to bind to both types of oligomer, 77 proteins were identified from an extensive literature search to be related to the inflammatory response (red squares points in Figure 5B), hence defining the proteins that could potentially be responsible for the inflammatory response observed in N13 microglia cells. The list of these proteins, which we define as the immune interactome, is shown in Table 1.

In order to identify the proteins involved in the immune response elicited in microglia, we compared the abundances of the membrane proteins found to interact with both types of oligomer in the whole oligomer interactome (see Materials and Methods for details), with the corresponding protein levels at which they are naturally present in microglial cells obtained from a recent MS proteomic study [47]. In Figure 5C, we report the abundances of membrane proteins bound to type B oligomers, compared to the abundances of the proteins in microglia, normalised as z-scores [47] and filtered for membrane localisation. Data from the type B oligomer binders were used as representative of abundance rankings of the proteins in the oligomer interactome since abundance rankings are conserved between oligomer types (Figure 4B) and the abundance values are more accurate from the analysis of the type B oligomer samples, because of the higher intensities of the MS signal.

We then sorted the proteins listed in Table 1 according to specific criteria to reveal a 'top ranked binders' selection: (i) proteins that are most abundant in the oligomer interactome, i.e. are in the top 10% of the abundance distribution; (ii) proteins binding to the oligomers that are found in the top 10% of the abundance distribution in the microglia and in the top 25% of the abundance distribution in the oligomer interactome, (iii) proteins that are observed to bind strongly to the oligomers despite their low abundance, i.e. those in the bottom 10% of the abundance protein distribution in microglia and at least average abundance in the oligomer interactome; (iv) proteins with the highest ratio of binding to type B relative to type A oligomers,

Table 1. The immune interactome. **List of the 77 membrane proteins found to bind to both type A and type B oligomers and known to be related to the immune response.**

Protein_IDs	Leading_ID	Entry name	Gene names	Protein names
Q922R8	Q922R8	PDIA6_MOUSE	Pdia6 Txndc7	Protein disulfide-isomerase A6 (EC 5.3.4.1)
P06800-3;P06800-2;P06800	P06800-3	PTPRC_MOUSE	Ptprc Ly-5	Receptor-type tyrosine-protein phosphatase C (EC 3.1.3.48)
O35658	O35658	C1QBP_MOUSE	C1qbp Gc1qbp	Complement component 1 Q subcomponent-binding protein
Q61830	Q61830	MRC1_MOUSE	Mrc1	Macrophage mannose receptor 1 (MMR) (CD antigen CD206)
Q9JJX6-4;Q9JJX6-2;Q9JJX6-3;Q9JJX6	Q9JJX6-4	P2RX4_MOUSE	P2rx4 P2x4	P2X purinoceptor 4 (P2X4)
Q91ZX7	Q91ZX7	LRP1_MOUSE	Lrp1 A2mr	Prolow-density lipoprotein receptor-related protein 1 (LRP-1) (Alpha-2-macroglobulin receptor) (A2MR) (CD antigen CD91)
Q61549	Q61549	AGRE1_MOUSE	Adgre1 Emr1 Gpf480	Adhesion G protein-coupled receptor E1 (Cell surface glycoprotein F4/80)
P17710-3;P17710-4;P17710-2;P17710	P17710-3	HXK1_MOUSE	Hk1	Hexokinase-1 (EC 2.7.1.1)
Q9Z0M6-2;Q9Z0M6-3;Q9Z0M6	Q9Z0M6-2	CD97_MOUSE	Cd97	CD97
P07901	P07901	HS90A_MOUSE	Hsp90aa1 Hsp86 Hsp86-1 Hspca	Heat shock protein HSP 90-alpha (Heat shock 86 kDa) (HSP 86) (HSP86)
O70172	O70172	PI42A_MOUSE	Pip4k2a Pip5k2a	Phosphatidylinositol 5-phosphate 4-kinase type-2 al-pha (EC 2.7.1.149
P41251	P41251	NRAM1_MOUSE	Slc11a1 Bcg Ity Lsh Nramp1	Natural resistance-associated macrophage protein 1 (NRAMP 1)
Q9WTR1	Q9WTR1	TRPV2_MOUSE	Trpv2 Grc	Transient receptor potential cation channel subfamily V member 2 (TrpV2)
P01899;P01897;P14430;P14429;P01896 ;P14431;P01898;P01902	P01899	HA11_MOUSE	H2-D1	H-2 class I histocompatibility antigen D-B alpha chain (H-2D(B))
B2RXS4	B2RXS4	PLXB2_MOUSE	Plxnb2	Plexin-B2
P21279;P21278	P21279	GNAQ_MOUSE	Gnaq	Guanine nucleotide-binding protein G(q) subunit alpha
Q8R422	Q8R422	CD109_MOUSE	Cd109	CD109 antigen (GPI-anchored alpha-2 macroglobulin-related protein
Q9QUN7	Q9QUN7	TLR2_MOUSE	Tlr2	Toll-like receptor 2 (CD antigen CD282)
Q922S4	Q922S4	PDE2A_MOUSE	Pde2a	cGMP-dependent 3',5'-cyclic phosphodiesterase (EC 3.1.4.17)
P63017;P17156	P63017	HSP7C_MOUSE	Hspa8 Hsc70 Hsc73	Heat shock cognate 71 kDa protein (Heat shock 70 kDa protein 8)
Q61093;Q8CIZ9-2;Q8CIZ9;Q8CIZ9-3	Q61093	CY24B_MOUSE	Cybb Cgd	Cytochrome b-245 heavy chain
P09581;O35942;Q6P5G0;Q62406;Q624 06-2;Q61532;Q78DX7	P09581	CSF1R_MOUSE	Csf1r Csfmr Fms	Macrophage colony-stimulating factor 1 receptor (CSF-1 receptor)
Q6A0D4	Q6A0D4	RFTN1_MOUSE	Rftn1 Kiaa0084	Raftlin (Raft-linking protein)
Q99JB2	Q99JB2	STML2_MOUSE	Stoml2 Slp2	Stomatin-like protein 2
Q61462;Q61462-2	Q61462	CY24A_MOUSE	Cyba	Cytochrome b-245 light chain
P20491	P20491	FCERG_MOUSE	Fcer1g Fce1g	High affinity immunoglobulin epsilon receptor subunit gamma (Fc receptor gamma-chain)
Q9D8Y0;Q9D4J1	Q9D8Y0	EFHD2_MOUSE	Efhd2 Sws1	EF-hand domain-containing protein D2 (Swiprosin-1)
P04441-2;P04441	P04441-2	HG2A_MOUSE	Cd74 Ii	H-2 class II histocompatibility antigen gamma chain (Ia antigen-associated invariant chain) (CD74)
Q6P9J9;Q6P9J9-2	Q6P9J9	ANO6_MOUSE	Ano6 Tmem16f	Anoctamin-6 (Small-conductance calcium-activated nonselective cation channel)
P28867;P28867-2;REV__Q6ZPL9	P28867	KPCD_MOUSE	Prkcd Pkcd	Protein kinase C delta type (EC 2.7.11.13)
Q80WJ7	Q80WJ7	LYRIC_MOUSE	Mtdh Lyric	Protein LYRIC (3D3/LYRIC)
Q8VDD8	Q8VDD8	WASH1_MOUSE	Wash1 Orf19 Wash	WAS protein family homolog 1
Q9D1D4;Q9D1D4-2	Q9D1D4	TMEDA_MOUS E	Tmed10 Tmp21	Transmembrane emp24 domain-containing protein 10
P62821	P62821	RAB1A_MOUSE	Rab1A Rab1	Ras-related protein Rab-1A
O70472	O70472	TM131_MOUSE	Tmem131 D1Bwg0491e Kiaa0257 Rw1	Transmembrane protein 131
P41233	P41233	ABCA1_MOUSE	Abca1 Abc1	ATP-binding cassette sub-family A member 1
P41241;P41242-3;P41242;P41242-2	P41241	CSK_MOUSE	Csk	Tyrosine-protein kinase CSK (EC 2.7.10.2)
P35991;Q60629;Q8CBF3-2;Q03145;P29319;Q8CBF3;P54761;Q61772-2;P54754;Q61772-3;P54763;P54763-2;Q61772;O09127;Q62413	P35991	BTK_MOUSE	Btk Bpk	Tyrosine-protein kinase BTK (EC 2.7.10.2)
Q9CQW9	Q9CQW9	IFM3_MOUSE	Ifitm3	Interferon-induced transmembrane protein 3 (Dispanin subfamily A member 2b)
Q9JKF1;Q3UQ44	Q9JKF1	IQGA1_MOUSE	Iqgap1	Ras GTPase-activating-like protein IQGAP1
Q9D3P8	Q9D3P8	PLRKT_MOUSE	Plgrkt	Plasminogen receptor (KT) (Plg-R(KT))

Q60875-5;Q60875-4;Q60875;Q60875-3;Q60875-2	Q60875-5	ARHG2_MOUSE	Arhgef2 Kiaa0651 Lbcl1 Lfc	Rho guanine nucleotide exchange factor 2
P70658-2;P70658	P70658-2	CXCR4_MOUSE	Cxcr4 Cmkar4 Lestr Sdf1r	C-X-C chemokine receptor type 4 (CXC-R4)
P04223-2;P04223;P06339;P14432	P04223-2	HA1K_MOUSE	H2-K1 H2-K	H-2 class I histocompatibility antigen
Q3TBT3;Q3TBT3-3;Q3TBT3-2	Q3TBT3	STING_MOUSE	Tmem173 Eris Mita Mpys Sting	Stimulator of interferon genes protein (mSTING)
P03991;P14428	P03991	HA1W_MOUSE	H2-K1 H2-K	H-2 class I histocompatibility antigen
Q6R5N8	Q6R5N8	TLR13_MOUSE	Tlr13	Toll-like receptor 13
P25911-2	P25911-2	LYN_MOUSE	Lyn	Tyrosine-protein kinase Lyn (EC 2.7.10.2)
P43406	P43406	ITAV_MOUSE	Itgav	Integrin alpha-V (Vitronectin receptor subunit alpha)
Q80TH2-1;Q80TH2;Q80TH2-2;Q80TE7	Q80TH2-1	LAP2_MOUSE	Erbb2ip Erbin Kiaa1225 Lap2	Protein LAP2 (Densin-180-like protein)
Q9QVP9	Q9QVP9	FAK2_MOUSE	Ptk2b Fak2 Pyk2 Raftk	Protein-tyrosine kinase 2-beta (EC 2.7.10.2)
P68181-4;P68181-2;P68181-3;P68181	P68181-4	KAPCB_MOUSE	Prkacb Pkacb	cAMP-dependent protein kinase catalytic subunit beta (PKA C-beta) (EC 2.7.11.11)
Q9JJ28	Q9JJ28	FLII_MOUSE	Flii Fli1 Fliih	Protein flightless-1 homolog
Q18PI6;Q18PI6-2;Q18PI6-3	Q18PI6	SLAF5_MOUSE	Cd84 Slamf5	SLAM family member 5 (Leukocyte differentiation antigen CD84)
Q64343	Q64343	ABCG1_MOUSE	Abcg1 Abc8 Wht1	ATP-binding cassette sub-family G member
P62482;P63143	P62482	KCAB2_MOUSE	Kcnab2 Ckbeta2 I2rf5 Kcnb3	Voltage-gated potassium channel subunit beta-2 (EC 1.1.1.-)
Q9WVK4;Q8BH64	Q9WVK4	EHD1_MOUSE	Ehd1 Past1	EH domain-containing protein 1 (PAST homolog 1) (mPAST1)
Q8BGU5-2;Q8BGU5	Q8BGU5-2	CCNY_MOUSE	Ccny Cfp1	Cyclin-Y (Cyclin fold protein 1)
P48025	P48025	KSYK_MOUSE	Syk ptk72 Sykb	Tyrosine-protein kinase SYK (EC 2.7.10.2)
Q8K4Q8	Q8K4Q8	COL12_MOUSE	Colec12 Clp1 Srcl	Collectin-12
P63158	P63158	HMGB1_MOUSE	Hmgb1 Hmg-1 Hmg1	High mobility group protein B1
P31996-2;P31996	P31996-2	CD68_MOUSE	Cd68	Macrosialin (CD68)
P25911;P16277	P25911	LYN_MOUSE	Lyn	Tyrosine-protein kinase Lyn (EC 2.7.10.2)
P49300	P49300	CLC10_MOUSE	Clec10a Mgl Mgl1	C-type lectin domain family 10 member A (MMGL)
P49769;Q61144-2;Q61144	P49769	PSN1_MOUSE	Psen1 Ad3h Psnl1	Presenilin-1 (PS-1) (EC 3.4.23.-)
Q61072	Q61072	ADAM9_MOUSE	Adam9 Kiaa0021 Mdc9 Mltng	Disintegrin and metalloproteinase domain-containing protein 9 (ADAM 9) (EC 3.4.24.-)
Q60766-2;Q60766	Q60766-2	IRGM1_MOUSE	Irgm1 Ifi1 Iigp3 Irgm	Immunity-related GTPase family M protein 1 (EC 3.6.5.-)
O54885	O54885	TYOBP_MOUSE	Tyrobp Dap12 Karap	TYRO protein tyrosine kinase-binding protein (DNAX-activation protein 12)
P05555-2;P05555	P05555-2	ITAM_MOUSE	Itgam	Integrin alpha-M (CD11 antigen-like family member B)
O88351	O88351	IKKB_MOUSE	Ikbkb Ikkb	Inhibitor of nuclear factor kappa-B kinase subunit beta (I-kappa-B-kinase beta)
Q8C863;Q8BZZ3;Q8C863-2	Q8C863	ITCH_MOUSE	Itch	E3 ubiquitin-protein ligase Itchy (EC 6.3.2.-)
Q99NH8;Q99NH8-2	Q99NH8	TREM2_MOUSE	Trem2 Trem2a Trem2b Trem2c	Triggering receptor expressed on myeloid cells 2 (TREM-2)
Q3U1F9	Q3U1F9	PHAG1_MOUSE	Pag1 Cbp Pag	Phosphoprotein associated with glycosphingolipid-enriched microdomains 1 (Csk-binding protein) (Transmembrane phosphoprotein Cbp)
Q08857	Q08857	CD36_MOUSE	Cd36	Platelet glycoprotein 4 (Glycoprotein IIIb)
Q3TD49-2;Q3TD49	Q3TD49-2	SPP2B_MOUSE	Sppl2b	Signal peptide peptidase-like 2B (SPP-like 2B) (SPPL2b) (EC 3.4.23.-)
Q9JJR8	Q9JJR8	TMM9B_MOUSE	Tmem9b	Transmembrane protein 9B
O88597	O88597	BECN1_MOUSE	Becn1	Beclin-1 (Coiled-coil myosin-like BCL2-interacting protein)

as the former are more effective in inducing cytokine release. These criteria allowed us to rank and screen the list of immune-related type B oligomer binders, and the resulting selection of the top ranked proteins is shown in Table 2. The list discloses proteins involved in cell signalling of particular relevance to the mechanisms of innate immunity.

DISCUSSION

Studies of the mechanisms of neurodegeneration associated with protein misfolding and aggregation has led to the conclusion that multiple lines of investigation are required to understand the multifactorial nature of such neuropathologies [9 48]. The inflammatory process associated with protein aggregation and deposition has been recognized to be a major contribution to the onset and progression of neurodegenerative misfolding diseases [15 16]. However, for a number of reasons, including the challenges involved in the structural characterisation of disease-linked protein oligomers, their low stability under experimental conditions, and the lack of comparative studies performed in parallel, there is still a lack of information related to correlations of oligomer structure and function. Such difficulties have limited the elucidation of crucial and common molecular mechanisms underlying oligomer-elicited immune responses in neurodegenerative diseases. As we have reported in this study, the HypF-N oligomer model enables one to overcome many of these constraints.

Our results from experiments involving the stimulation of microglial cells using type A and B oligomers of HypF-N showed that both types of oligomer stimulate the release of pro-inflammatory cytokines, validating the use of the

Table 2. Highest ranked immune-related candidates. Selection of the highest ranked immune-related proteins identified in the type B oligomer interactome according to the selection criteria i-iv discussed in the text. The proteins highlighted in the list are those matching two or more selection criteria. The proteins ID and name, gene names and experimental values of binding ratio for type B oligomers vs type A oligomers (log2(B/A)), the proportion of a given protein in the type B oligomer sample (log10(% in B)), proportion of the protein in the type A oligomer sample (log10(% in A)), and in microglia (log10(% in microglia)) are indicated.

CRITERIA[a]	Leading ID	Gene names	log2(B/A)	log10(% in B)	log10(% in A)	log10(% in microglia)	Protein names
(i)	P63017	Hspa8 Hsc70 Hsc73	2.6	-0.48	-0.75	-0.276	Heat shock cognate 71 kDa protein (Heat shock 70 kDa protein 8)
	P62821	Rab1A Rab1	1.8	-0.534	-0.601	-0.855	Ras-related protein Rab-1A (YPT1-related protein)
	P20491	Fcer1g Fce1g	2.37	-0.89	-1.1	-	High affinity immunoglobulin epsilon receptor subunit gamma (Fc receptor gamma-chain)
	Q9JKF1	Iqgap1	1.34	-0.976	-0.94	-0.326	Ras GTPase-activating-like protein IQGAP1
	Q922R8	Pdia6 Txndc7	6.66	-1.07	-2.11	-0.699	Protein disulfide-isomerase A6 (EC 5.3.4.1)
	Q61462	Cyba	2.4	-1.21	-1.38	-2.474	Cytochrome b-245 light chain
	P07901	Hsp90aa1 Hsp86 Hsp86-1 Hspca	3.79	-1.25	-1.9	-0.959	Heat shock protein HSP 90-alpha (Heat shock 86 kDa)
	Q99JB2	Stoml2 Slp2	2.42	-1.26	-1.46	-2.046	Stomatin-like protein 2
	Q80WJ7	Mtdh Lyric	2.11	-1.29	-1.47	-1.687	Protein LYRIC (3D3/LYRIC)
	O35658	C1qbp Gc1qbp	4.97	-1.29	-2.36	-1.266	Complement component 1 Q subcomponent-binding protein
	Q61093	Cybb Cgd	2.57	-1.38	-1.7	-1.589	Cytochrome b-245 heavy chain
	Q9CQW9	Ifitm3	1.42	-1.47	-1.44	-1.75	Interferon-induced transmembrane protein 3
	Q9D3P8	Plgrkt	1.21	-1.54	-1.46	-2.09	Plasminogen receptor (KT) (Plg-R(KT))
	P01899	H2-D1	3.15	-1.65	-2.06	-2.74	H-2 class I histocompatibility antigen, D-B alpha chain (H-2D(B))
	P41251	Slc11a1 Bcg Ity Lsh Nramp1	3.43	-1.67	-2.02	-2.57	Natural resistance-associated macrophage protein 1 (NRAMP 1)
	Q6A0D4	Rftn1 Kiaa0084	2.48	-1.72	-1.91	-2.6	Raftlin (Raft-linking protein)
	Q9D8Y0	Efhd2 Sws1	2.22	-1.78	-1.96	-1.18	EF-hand domain-containing protein D2 (Swiprosin-1)
(ii)	Q8R422	Cd109	3.08	-2.34	-2.76	-4.558	CD109 antigen (GPI-anchored alpha-2 macroglobulin-related protein)
	P25911-2	Lyn	2.21	-2.5	-2.55	-3.301	Tyrosine-protein kinase Lyn (EC 2.7.10.2)
	P62482	Kcnab2 Ckbeta2 I2rf5 Kcnb3	1.33	-1.74	-1.66	-3.482	Voltage-gated potassium channel subunit beta-2 (EC 1.1.1.-)
(iii)	Q922R8	Pdia6 Txndc7	6.66	-1.07	-2.11	-0.699	Protein disulfide-isomerase A6 (EC 5.3.4.1)
	P06800-3	Ptprc Ly-5	5.42	-2.18	-3.05	-0.969	Receptor-type tyrosine-protein phosphatase C (EC 3.1.3.48)
	O35658	C1qbp Gc1qbp	4.97	-1.29	-2.36	-1.266	Complement component 1 Q subcomponent-binding protein
	Q61830	Mrc1	4.93	-2.57	-3.04	-0.673	macrophage mannose receptor 1 (MMR)
	Q9JJX6-4	P2rx4 P2x4	4.58	-2.26	-2.93	-1.921	P2X purinoceptor 4 (P2X4)
	Q61549	Adgre1 Emr1 Gpf480	4.12	-2.28	-2.95	-2.28	Adhesion G protein-coupled receptor E1 (Cell surface glycoprotein F4/80)
	P17710-3	Hk1	4.11	-3.11	-3.67	-1.555	Hexokinase-1 (EC 2.7.1.1)
	Q9Z0M6-2	Cd97	3.99	-2.48	-2.88	-3.302	CD97
	P07901	Hsp90aa1 Hsp86 Hsp86-1 Hspca	3.79	-1.25	-1.9	-0.959	Heat shock protein HSP 90-alpha (Heat shock 86 kDa)
	O70172	Pip4k2a Pip5k2a	3.76	-2.26	-2.8	-1.92	Phosphatidylinositol 5-phosphate 4-kinase type-2 alpha (EC 2.7.1.149)
	P41251	Slc11a1 Bcg Ity Lsh Nramp1	3.43	-1.67	-2.02	-2.57	Natural resistance-associated macrophage protein 1 (NRAMP 1)
	Q9WTR1	Trpv2 Grc	3.37	-2.06	-2.44	-1.982	Transient receptor potential cation channel subfamily V member 2 (TrpV2)
(iv)	P04441-2	Cd74 Ii	2.19	-2.06	-2.21	-3.019	H-2 class II histocompatibility antigen gamma chain (Ia antigen-associated invariant chain)
	Q9QUN7	Tlr2	2.95	-2.6	-2.85	-1.41	Toll-like receptor 2 (CD antigen CD282)

a Criteria as defined in the text

HypF-N oligomers as a model of neuroinflammation induced by protein misfolding [14 29]. We note that the stimulation of cytokine release was observed following exposure to very low concentrations of oligomers, as many as three orders of magnitude lower than those needed to cause detectable cytotoxicity, suggesting the importance of this phenomenon at early stages of pathology, when the concentration of misfolded protein oligomers is still very low. Interestingly, when the ability of type A and type B oligomers to stimulate the immune response was evaluated within the lower concentration range, type B oligomers were found to be stronger inducers of pro-inflammatory cytokine release than type A oligomers. As the

surfaces of type B oligomers are less hydrophobic than those of type A oligomers, these results suggest that hydrophobicity may not be the dominant determinant feature that triggers innate immunity, as previously proposed using other protein systems [23] [24], but that other more specific binding properties may be important in determining the magnitude of the oligomer-elicited immune response.

The explanation of this phenomenon seems to reside in the different capability of both oligomer types to interact with the protein and lipid components of the cell. Indeed, through the analysis of confocal microscopy images, type A oligomers were found to interact and penetrate the cell membrane of microglial cells, consistent with their higher hydrophobicity and in agreement with previous data acquired on cultured SH-SY5Y neuroblastoma cells [2] [39]. This phenomenon is a result of the ability of these species to interact with, and destabilize, the lipid bilayer of the membrane [49]. By contrast, type B aggregates were found primarily to remain attached to the cell surface without penetrating the lipid bilayer, as found previously for neuronal cells [2] [39]. Indeed, type B, unlike type A oligomers, were found to be unable to interact with a supported lipid bilayer reconstituted in the absence of membrane proteins [49].

The pull-down assays and mass spectrometry data presented here have in addition revealed that type B oligomers bind more strongly to membrane proteins than do type A oligomers. This higher overall affinity for proteins of type B, compared to type A oligomers, is likely to arise from the lower degree of solvent-exposed hydrophobic regions of the former species that makes their surfaces more hydrophilic. In fact, it is well established that both cytosolic proteins and extracellular domains of membrane proteins are also hydrophilic as they bury their hydrophobic patches on the interior and therefore are likely to have a higher affinity for type B than type A oligomers. This affinity could also be enhanced by their greater dynamic nature of their structure [22] and indeed this characteristic is a parameter that is taken into consideration in the rationalization of protein-protein interactions [50] [51]. This higher affinity of type B relative to type A species for membrane proteins would be likely to lead to more favourable interactions with protein receptors on the cell surface, hence enabling more effective activation of immune signalling and cytokine release (Figure 6).

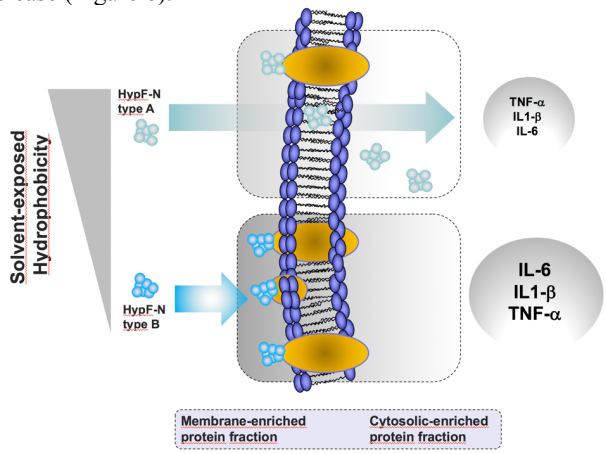

Figure 6. Summary of the detected interactions of type A and type B oligomers with microglial cells. **The cartoon illustrates the differential hydrophobic nature, subcellular localisation, protein binding capability and cytokine release outcome of the two types of oligomers.**

The membrane proteins to which the oligomers interact most strongly, and so are most likely to be involved in this immune response, were identified by a systematic high-throughput proteomic analysis, resulting in the identification of 77 immune-related proteins that bind strongly to the oligomers. Of particular interest is that a number of those proteins (Table 1) have been recently suggested to be involved in microglial responses in the context of amyloid disease, notably TREM2, CD36 (regulators of phagocytosis), HMGB1, presenilin-1, beclin-1, and Lrp1/CD91 [52] [53] [54] [55] (Table 1), as well as TLR2 and PTPRC/CD45 [56] [5758] (Tables 1 and 2). In addition to these proteins, which have been associated with inflammatory responses linked to neurodegenerative disease, our data reveal a number of previously unidentified candidates involved in oligomer-elicited innate immunity, including Efhd2/swiprosin-1, CD74, PDIA6, P2X4, C1qbp, CD68, CD97, Mrc1/MMR, FcεRI, and Plgrkt (Tables 1 and 2) and CD84 (Table 1) receptor proteins. Furthermore, a number of heat-shock proteins (HSPA8/HSC70, HSPCA/HSP90), signalling kinases (Lyn, Plp4k2a, CSK, Syk and NFκB inhibitor Ikkb) and other signalling (e.g. Mtdh/LYRIC) or protein-stabilizing (ubiquitin-E3 ligase Itch) molecules with potential roles in the oligomers-elicited immune response have also been identified.

In conclusion, the detailed definition of the interactomes of two well-characterized oligomers from the highly amyloidogenic protein HypF-N, having a different hydrophobic character and with differential protein binding capacities and neuroinflammatory capabilities, contributes to the elucidation of the primary determinants of cellular recognition of misfolded protein misfolded oligomers, and of their effects in eliciting the innate immunity responses that are associated with protein misfolding diseases.

EXPERIMENTAL SECTION

Preparation of HypF-N oligomers. Protein expression and purification were carried out as described previously [2]. Incubation of the purified native protein with polymixin B to eliminate possible bacterial endotoxins was performed as previously described [59]. The content of endotoxins in HypF-N protein solution samples was determined by toxin sensor Limulus Amebocyte Lysate (LAL) assay kit (Genscript, Piscataway, NJ) and resulted to be <1 EU/mg of protein. Type A and type B oligomeric aggregates of HypF-N were prepared by incubating the protein for 4 h at 25 °C and at a concentration of 48 μM in two different experimental conditions: (i) 50 mM acetate buffer, 12% (v/v) TFE, 2 mM DTT, pH 5.5 (condition A) and (ii) 20 mM TFA, 330 mM NaCl, pH 1.7 (condition B) [2]. The oligomers were centrifuged at 16,100 g for 10 min and resuspended in PBS buffer or in cell culture medium.

Cell cultures. Murine N13 microglia cells were cultured in Dulbecco's Modified Eagle's Medium (DMEM) F12 supplemented with 10% fetal bovine serum (FBS), 1.0% non-essential amino acids, glutamine and antibiotics. The cell culture was maintained in a 5.0% CO2 humidified atmosphere at 37 °C and grown until 80% confluence for a maximum of 20 passages.

MTT reduction assay. The type A and type B oligomers were resuspended in cell culture medium at a corresponding

monomer concentration ranging from 0.005 μM to 12 μM and exogenously added to the cells. The viability of the cells was assessed after 24 h through the MTT assay using the Cell Proliferation Kit I (MTT) (Roche, Mannheim, Germany) according to the manufacturer's protocol. Absorbance values of blue formazan were determined at 575 nm and cell viability was expressed as percent of MTT reduction in treated cells as compared to untreated cells (assumed as 100%). Data were expressed as mean ± standard error of the mean (SEM). Comparisons between group pairs were performed using the Student's t test and a p-value lower than 0.05 was considered statistically significant.

Cytokine release measurements. The type A and type B oligomers were resuspended in cell culture medium at a concentration ranging from 0.005 μM to 12 μM (monomer equivalents) and extracellularly added to the cells. Non-aggregated HypF-N protein was also used in the same experimental setting at different concentrations. LPS at a concentration of 1 μg/ml, and culture medium alone were used as positive and negative controls, respectively. The incubation lasted 6 h for TNF-α and 24 h for IL-6, IL-1β and IL-10 release measurements. Cell culture supernatants were harvested and centrifuged at 400 g for 5 min and cell-cleared supernatants were assayed through ELISA to check the levels of IL-6, IL-1β, TNF-α and IL-10, using Mouse IL-6/IL-1β/TNF-α/IL-10 BD OptEIA ELISA set (BD Biosciences, Madrid, Spain) according to the manufacturer's protocol. Data were expressed as mean ± SEM. Comparisons between group pairs were performed using the Student's t test. A p-value lower than 0.05 was considered statistically significant.

Immunofluorescence confocal microscopy. N13 cells were seeded on glass coverslips and incubated for 24 h with type A and type B oligomers added extracellularly at a corresponding monomer concentration of 0.7 μM. The cells were subjected to intensive washing with PBS, and then fixed in 2% (w/v) buffered paraformaldehyde for 15 min at 4 °C. The first and second halves of the coverslips were treated for 1 h at 4 °C with a PBS solution containing 3% BSA (w/v) with and without 0.5% (v/v) Triton X-100 to allow plasma membrane permeabilization and leave the cells unpermeabilised, respectively. The coverslips were incubated overnight with 1:1000 diluted rabbit polyclonal anti-HypF-N antibodies (Primm, Milan, Italy) and then for 1 h at room temperature in the dark with 1:800 diluted Alexa Fluor 633-conjugated anti-rabbit secondary antibodies (Thermo Fisher Scientific, Waltham, MA). The nuclei were stained with 1 μg/ml DAPI for 5 min at room temperature. Confocal scanning microscope images were acquired using a Leica TCS SP5 confocal scanning microscope (Mannheim, Germany) at 40x or 63x magnification from randomly chosen fields. Images were analyzed using the cell counter plugin of the image analysis program ImageJ (NIH, Bethesda, MD, U.S.A.).

Protein pull-down assays. Proteins from N13 cell cultures were extracted and membrane-enriched using the ProteoExtract Native Membrane Protein Extraction Kit (Calbiochem, Darmstadt, Germany) according to the manufacturer's protocol. 10,000,000 cell/ml of microglial cell lysate and 24 μM (monomer equivalents) type A or type B oligomers were incubated in isolation or in combination in a final volume of 400 μL for 1 h at 37 °C under gentle shaking and then centrifuged at 16,100 g for 10 min. Aliquots of the pellet fractions were subjected to SDS-PAGE using 4-12% Bis-Tris polyacrylamide gels.

Mass spectrometry-based (GeLC MS/MS) proteomic analysis. 1D gel bands were excised and transferred into a 96-well PCR plate. The gel bands were cut into 1 mm2 pieces, destained, reduced (DTT) and alkylated (iodoacetamide) and subjected to enzymatic digestion with trypsin overnight at 37 °C. After digestion, the supernatant was pipetted into a sample vial and loaded onto an autosampler for automated LC-MS/MS analysis. All LC-MS/MS experiments were performed using a nanoAcquity UPLC (Waters Corp., Milford, MA) system and an LTQ Orbitrap Velos hybrid ion trap mass spectrometer (Thermo Scientific, Waltham, MA). Separation of peptides was performed by reverse-phase chromatography using a Waters reverse-phase nano column (BEH C18, 75 μm i.d. x 250 mm, 1.7 μm particle size) at flow rate of 300 nL/min. Peptides were initially loaded onto a pre-column (Waters UPLC Trap Symmetry C18, 180 μm i.d. x 20 mm, 5 μm particle size) from the nanoAcquity sample manager with 0.1% formic acid for 3 min at a flow rate of 5 μL/min. After this period, the column valve was switched to allow the elution of peptides from the pre-column onto the analytical column. Solvent A was water + 0.1% formic acid and solvent B was acetonitrile + 0.1% formic acid. The linear gradient employed was 3-30% B in 40 min (the total run time, including wash/equilibration steps was 60 min). The LC eluent was sprayed into the mass spectrometer by means of a nanospray ion source. All m/z values of eluting ions were measured in the Orbitrap Velos mass analyzer, set at a resolution of 30000 and scanned from m/z 380-1500. Data dependent scans (Top 20) were employed to automatically isolate and generate fragment ions by collision-induced dissociation (NCE:30%) in the linear ion trap, resulting in the generation of MS/MS spectra. Ions with charge states of 2+ and above were selected for fragmentation.

GeLC MS/MS data analysis. Post-run, the data were processed using the MaxQuant software (version 1.5.3.17) for protein identification and quantification [6061], using default settings and proteins were searched against the SwissProt Mouse database (03 September 2015, consisting of 24747 sequences) [46]. The false discovery rate for proteins and peptides was set to 1% with the specified UniProt database in decoy mode, and the option 'match between runs' was enabled. Values of absolute protein abundances (iBAQ) were obtained in each of the four biological replicas. Median values among the iBAQ intensities per replica were used to average the protein abundance within each condition. Z-scored normalisation was then applied to the averaged abundance distribution of proteins in order to rank the proteins in the sample in terms of abundance for direct comparison with abundances in another condition. This transformation normalises the abundance distribution by shifting the average value to 0 and rescaling the standard deviation to 1. This approach allows different abundance distributions to be aligned in the same range, for ranking comparisons. The same procedure was used for the available MS-based proteomics data of proteins abundances (iBAQ values, three biological replica) in microglia cells from Sharma and coworkers [47].

ASSOCIATED CONTENT

Supporting Information

The Supporting Information is available free of charge on the ACS Publications website.

AUTHOR INFORMATION

Corresponding Author

* cmd44@cam.ac.uk; david.pozo@cabimer.es; cintia.roodveldt@cabimer.es

Author Contributions

BM and CR designed research; BM and ALG performed experimental research; GV and BF analysed mass spectrometry data; BM, GV, ALG, BF, KL, DP, MV, FC, CMD and CR analysed data and wrote the paper.

Funding Sources

Financial support was provided by FEBS (Short-Term Fellowship to BM), EMBO (ASTF 450-2013 Short-Term Fellowships to BM), the Spanish Ministry of Economy (RTC-2015-3309-1 to CR; ISCIII CPII16/58 to CR and PI14-1600 to DP), the Regional Ministry of Economy (P11-CTS-8161 and PAIDI2020 CTS-677 to DP), and Programa 'Atracción de Talento', University of Seville (to CR). This work was also supported by the Cambridge Centre for Misfolding Diseases (BM, GV, MV, CMD).

REFERENCES

(1) Chiti, F.; Dobson, C. M. Protein Misfolding, Amyloid Formation, and Human Disease: A Summary of Progress over the Last Decade. *Annu. Rev. Biochem.* **2017**, *86* (1), 27–68.

(2) Campioni, S.; Mannini, B.; Zampagni, M.; Pensalfini, A.; Parrini, C.; Evangelisti, E.; Relini, A.; Stefani, M.; Dobson, C. M.; Cecchi, C.; et al. A Causative Link between the Structure of Aberrant Protein Oligomers and Their Toxicity. *Nat. Chem. Biol.* **2010**, *6* (2), 140–147.

(3) Fusco, G.; Chen, S. W.; Williamson, P. T. F.; Cascella, R.; Perni, M.; Jarvis, J. A.; Cecchi, C.; Vendruscolo, M.; Chiti, F.; Cremades, N.; et al. Structural Basis of Membrane Disruption and Cellular Toxicity by α-Synuclein Oligomers. *Science (80-.).* **2017**, *358* (6369), 1440–1443.

(4) Olzscha, H.; Schermann, S. M.; Woerner, A. C.; Pinkert, S.; Hecht, M. H.; Tartaglia, G. G.; Vendruscolo, M.; Hayer-Hartl, M.; Hartl, F. U.; Vabulas, R. M. Amyloid-like Aggregates Sequester Numerous Metastable Proteins with Essential Cellular Functions. *Cell* **2011**, *144* (1), 67–78.

(5) Roodveldt, C.; Bertoncini, C. W.; Andersson, A.; van der Goot, A. T.; Hsu, S.-T.; Fernández-Montesinos, R.; de Jong, J.; van Ham, T. J.; Nollen, E. a; Pozo, D.; et al. Chaperone Proteostasis in Parkinson's Disease: Stabilization of the Hsp70/Alpha-Synuclein Complex by Hip. *EMBO J.* **2009**, *28* (23), 3758–3770.

(6) Balch, W. E.; Morimoto, R. I.; Dillin, A.; Kelly, J. W. Adapting Proteostasis for Disease Intervention. *Science* **2008**, *319* (5865), 916–919.

(7) Bence, N. F.; Sampat, R. M.; Kopito, R. R. Impairment of the Ubiquitin-Proteasome System by Protein Aggregation. *Science* **2001**, *292* (5521), 1552–1555.

(8) Gidalevitz, T.; Ben-Zvi, A.; Ho, K. H.; Brignull, H. R.; Morimoto, R. I. Progressive Disruption of Cellular Protein Folding in Models of Polyglutamine Diseases. *Science* **2006**, *311* (5766), 1471–1474.

(9) Mangialasche, F.; Solomon, A.; Winblad, B.; Mecocci, P.; Kivipelto, M. Alzheimer's Disease: Clinical Trials and Drug Development. *Lancet Neurol.* **2010**, *9* (7), 702–716.

(10) Karran, E.; Mercken, M.; Strooper, B. De. The Amyloid Cascade Hypothesis for Alzheimer's Disease: An Appraisal for the Development of Therapeutics. *Nat. Rev. Drug Discov.* **2011**, *10* (9), 698–712.

(11) Habchi, J.; Chia, S.; Limbocker, R.; Mannini, B.; Ahn, M.; Perni, M.; Hansson, O.; Arosio, P.; Kumita, J. R.; Challa, P. K.; et al. Systematic Development of Small Molecules to Inhibit Specific Microscopic Steps of Aβ42 Aggregation in Alzheimer's Disease. *Proc. Natl. Acad. Sci.* **2017**, *114* (2), E200–E208.

(12) Kim, Y. S.; Joh, T. H. Microglia, Major Player in the Brain Inflammation: Their Roles in the Pathogenesis of Parkinson's Disease. *Exp. Mol. Med.* **2006**, *38* (4), 333–347.

(13) McGeer, P. L.; Rogers, J.; McGeer, E. G. Inflammation, Anti-Inflammatory Agents and Alzheimer Disease: The Last 12 Years. *J. Alzheimer's Dis.* **2006**, *9*, 271–276.

(14) Masters, S. L.; O'Neill, L. A. J. Disease-Associated Amyloid and Misfolded Protein Aggregates Activate the Inflammasome. *Trends Mol. Med.* **2011**, *17* (5), 276–282.

(15) Ransohoff, R. M. How Neuroinflammation Contributes to Neurodegeneration. *Science* **2016**, *353* (6301), 777–783.

(16) Heneka, M. T.; Kummer, M. P.; Latz, E. Innate Immune Activation in Neurodegenerative Disease. *Nat. Rev. Immunol.* **2014**, *14* (7), 463–477.

(17) Bemporad, F.; Chiti, F. Protein Misfolded Oligomers: Experimental Approaches, Mechanism of Formation, and Structure-Toxicity Relationships. *Chem. Biol.* **2012**, *19* (3), 315–327.

(18) Cizas, P.; Budvytyte, R.; Morkuniene, R.; Moldovan, R.; Broccio, M.; Lösche, M.; Niaura, G.; Valincius, G.; Borutaite, V. Size-Dependent Neurotoxicity of β-Amyloid Oligomers. *Arch. Biochem. Biophys.* **2010**, *496* (2), 84–92.

(19) Ladiwala, A. R. A.; Litt, J.; Kane, R. S.; Aucoin, D. S.; Smith, S. O.; Ranjan, S.; Davis, J.; Van Nostrand, W. E.; Tessier, P. M. Conformational Differences between Two Amyloid β Oligomers of Similar Size and Dissimilar Toxicity. *J. Biol. Chem.* **2012**, *287* (29), 24765–24773.

(20) Cremades, N.; Cohen, S. I. A.; Deas, E.; Abramov, A. Y.; Chen, A. Y.; Orte, A.; Sandal, M.; Clarke, R. W.; Dunne, P.; Aprile, F. A.; et al. Direct Observation of the Interconversion of Normal and Toxic Forms of α-Synuclein. *Cell* **2012**, *149* (5), 1048–1059.

(21) Mannini, B.; Mulvihill, E.; Sgromo, C.; Cascella, R.; Khodarahmi, R.; Ramazzotti, M.; Dobson, C. M.; Cecchi, C.; Chiti, F. Toxicity of Protein Oligomers Is Rationalized by a Function Combining Size and Surface Hydrophobicity. *ACS Chem. Biol.* **2014**, *9* (10), 2309–2317.

(22) Capitini, C.; Patel, J. R.; Natalello, A.; D'Andrea, C.; Relini, A.; Jarvis, J. A.; Birolo, L.; Peduzzo, A.; Vendruscolo, M.; Matteini, P.; et al. Structural Differences between Toxic and Nontoxic HypF-N Oligomers. *Chem. Commun.* **2018**, *54* (62), 8637–8640.

(23) Seong, S.-Y.; Matzinger, P. Hydrophobicity: An Ancient Damage- Associated Molecular Pattern That Initiates Innate Immune Responses. *Nat. Rev. Immunol.* **2004**, *4* (6), 469–478.

(24) Moyano, D. F.; Goldsmith, M.; Solfiell, D. J.; Landesman-Milo, D.; Miranda, O. R.; Peer, D.; Rotello, V. M. Nanoparticle Hydrophobicity Dictates Immune Response. *J. Am. Chem. Soc.* **2012**, *134* (9), 3965–3967.

(25) Bolognesi, B.; Kumita, J. R.; Pereira de Barros, T.; Esbjorner, E. K.; Luheshi, L. M.; Crowther, D. C.; Wilson, M. R.; Dobson, C. M.; Favrin, G.; Yerbury, J. J. ANS Binding Reveals Common Features of Cytotoxic Amyloid Species. *ACS Chem. Biol.* **2010**, *5* (8), 735–740.

(26) Zhang, W.; Wang, T.; Pei, Z.; Miller, D. S.; Wu, X.; Block, M. L.; Wilson, B.; Zhang, W.; Zhou, Y.; Hong, J. Aggregated α-Synuclein Activates Microglia: A Process Leading to Disease Progression in Parkinson's Disease. *FASEB J.* **2005**, *19* (6), 533–542.

(27) Salminen, A.; Ojala, J.; Suuronen, T.; Kaarniranta, K.; Kauppinen, A. Amyloid-β Oligomers Set Fire to Inflammasomes and Induce Alzheimer's Pathology. *J. Cell. Mol. Med.* **2008**, *12* (6A), 2255–2262.

(28) Roberts, K.; Zeineddine, R.; Corcoran, L.; Li, W.; Campbell, I. L.; Yerbury, J. J. Extracellular Aggregated Cu/Zn Superoxide Dismutase Activates Microglia to Give a Cytotoxic Phenotype. *Glia* **2013**, *61* (3), 409–419.

(29) Leal-Lasarte, M. M.; Franco, J. M.; Labrador-Garrido, A.; Pozo, D.; Roodveldt, C. Extracellular TDP-43 Aggregates Target MAPK/MAK/MRK Overlapping Kinase (MOK) and Trigger Caspase-3/IL-18 Signaling in Microglia. *FASEB J.* **2017**, *31* (7), 2797–2816.

(30) Campioni, S.; Mossuto, M. F.; Torrassa, S.; Calloni, G.; de Laureto, P. P.; Relini, A.; Fontana, A.; Chiti, F. Conformational Properties of the Aggregation Precursor State of HypF-N. *J. Mol. Biol.* **2008**, *379* (3), 554–567.

(31) Chiti, F.; Bucciantini, M.; Capanni, C.; Taddei, N.; Dobson, C. M.; Stefani, M. Solution Conditions Can Promote Formation of Either Amyloid Protofilaments or Mature Fibrils from the HypF N-Terminal Domain. *Protein Sci.* **2001**, *10* (12), 2541–2547.

(32) Marcon, G.; Plakoutsi, G.; Canale, C.; Relini, A.; Taddei, N.; Dobson, C. M.; Ramponi, G.; Chiti, F. Amyloid Formation from HypF-N under Conditions in Which the Protein Is Initially in Its Native State. *J. Mol. Biol.* **2005**, *347* (2), 323–335.

(33) Relini, A.; Torrassa, S.; Rolandi, R.; Gliozzi, A.; Rosano, C.; Canale, C.; Bolognesi, M.; Plakoutsi, G.; Bucciantini, M.; Chiti, F.; et al. Monitoring the Process of HypF Fibrillization and Liposome Permeabilization by Protofibrils. *J. Mol. Biol.* **2004**, *338* (5), 943–957.

(34) Bucciantini, M.; Giannoni, E.; Chiti, F.; Baroni, F.; Formigli, L.; Zurdo, J.; Taddei, N.; Ramponi, G.; Dobson, C. M.; Stefani, M. Inherent Toxicity of Aggregates Implies a Common Mechanism for Protein Misfolding Diseases. *Nature* **2002**, *416* (6880), 507–511.

(35) Bucciantini, M.; Calloni, G.; Chiti, F.; Formigli, L.; Nosi, D.; Dobson, C. M.; Stefani, M. Prefibrillar Amyloid Protein Aggregates Share Common Features of Cytotoxicity. *J. Biol. Chem.* **2004**, *279* (30), 31374–31382.

(36) Cecchi, C.; Baglioni, S.; Fiorillo, C.; Pensalfini, A.; Liguri, G.; Nosi, D.; Rigacci, S.; Bucciantini, M.; Stefani. Insights into the Molecular Basis of the Differing Susceptibility of Varying Cell Types to the Toxicity of Amyloid Aggregates. *J. Cell Sci.* **2005**, *118* (15), 3459–3470.

(37) Evangelisti, E.; Cecchi, C.; Cascella, R.; Sgromo, C.; Becatti, M.; Dobson, C. M.; Chiti, F.; Stefani, M. Membrane Lipid Composition and Its Physicochemical Properties Define Cell Vulnerability to Aberrant Protein Oligomers. *J. Cell Sci.* **2012**, *125*, 2416–2427.

(38) Mannini, B.; Cascella, R.; Zampagni, M.; van Waarde-Verhagen, M.; Meehan, S.; Roodveldt, C.; Campioni, S.; Boninsegna, M.; Penco, A.; Relini, A.; et al. Molecular Mechanisms Used by Chaperones to Reduce the Toxicity of Aberrant Protein Oligomers. *Proc. Natl. Acad. Sci. U. S. A.* **2012**, *109* (31), 12479–12484.

(39) Zampagni, M.; Cascella, R.; Casamenti, F.; Grossi, C.; Evangelisti, E.; Wright, D.; Becatti, M.; Liguri, G.; Mannini, B.; Campioni, S.; et al. A Comparison of the Biochemical Modifications Caused by Toxic and Non-Toxic Protein Oligomers in Cells. *J. Cell. Mol. Med.* **2011**, *15* (10), 2106–2116.

(40) Baglioni, S.; Casamenti, F.; Bucciantini, M.; Luheshi, L. M.; Taddei, N.; Chiti, F.; Dobson, C. M.; Stefani, M. Prefibrillar Amyloid Aggregates Could Be Generic Toxins in Higher Organisms. *J. Neurosci.* **2006**, *26* (31), 8160–8167.

(41) Tatini, F.; Pugliese, A. M.; Traini, C.; Niccoli, S.; Maraula, G.; Ed Dami, T.; Mannini, B.; Scartabelli, T.; Pedata, F.; Casamenti, F.; et al. Amyloid-β Oligomer Synaptotoxicity Is Mimicked by Oligomers of the Model Protein HypF-N. *Neurobiol. Aging* **2013**, *34* (9), 2100–2109.

(42) Cascella, R.; Conti, S.; Mannini, B.; Li, X.; Buxbaum, J. N.; Tiribilli, B.; Chiti, F.; Cecchi, C. Transthyretin Suppresses the Toxicity of Oligomers Formed by Misfolded Proteins in Vitro. *Biochim. Biophys. Acta - Mol. Basis Dis.* **2013**, *1832* (12), 2302–2314.

(43) Saridaki, T.; Zampagni, M.; Mannini, B.; Evangelisti, E.; Taddei, N.; Cecchi, C.; Chiti, F. Glycosaminoglycans (GAGs) Suppress the Toxicity of HypF-N Prefibrillar Aggregates. *J. Mol. Biol.* **2012**, *421* (4–5), 616–630.

(44) Kettenmann, H.; Hanisch, U.-K.; Noda, M.; Verkhratsky, A. Physiology of Microglia. *Physiol. Rev.* **2011**, *91* (2), 461–553.

(45) Oliver, C.; Jamur, M. C. *Immunocytochemical Methods and Protocols*; 2009; Vol. 588.

(46) Bateman, A.; Martin, M. J.; O'Donovan, C.; Magrane, M.; Alpi, E.; Antunes, R.; Bely, B.; Bingley, M.; Bonilla, C.; Britto, R.; et al. UniProt: The Universal Protein Knowledgebase. *Nucleic Acids Res.* **2017**, *45* (D1), D158–D169.

(47) Sharma, K.; Schmitt, S.; Bergner, C. G.; Tyanova, S.; Kannaiyan, N.; Manrique-Hoyos, N.; Kongi, K.; Cantuti, L.; Hanisch, U. K.; Philips, M. A.; et al. Cell Type- and Brain Region-Resolved Mouse Brain Proteome. *Nat. Neurosci.* **2015**, *18* (12), 1819–1831.

(48) Talwar, P.; Sinha, J.; Grover, S.; Rawat, C.; Kushwaha, S.; Agarwal, R.; Taneja, V.; Kukreti, R. Dissecting Complex and Multifactorial Nature of Alzheimer's Disease Pathogenesis: A Clinical, Genomic, and Systems Biology Perspective. *Mol. Neurobiol.* **2016**, *53* (7), 4833–4864.

(49) Oropesa-Nuñez, R.; Keshavan, S.; Dante, S.; Diaspro, A.; Mannini, B.; Capitini, C.; Cecchi, C.; Stefani, M.; Chiti, F.; Canale, C. Toxic HypF-N Oligomers Selectively Bind the Plasma Membrane to Impair Cell Adhesion Capability. *Biophys. J.* **2018**, *114* (6), 1357–1367.

(50) Alvarez-Garcia, D.; Barril, X. Relationship between Protein Flexibility and Binding: Lessons for Structure-Based Drug Design. *J. Chem. Theory Comput.* **2014**, *10* (6), 2608–2614.

(51) Spyrakis, F.; Bidon Chanal, A.; Barril, X.; Luque, F. J. Protein Flexibility and Ligand Recognition: Challenges for Molecular Modeling. *Curr. Top. Med. Chem.* **2011**, *11* (2), 192–210.

(52) Hickman, S.; Izzy, S.; Sen, P.; Morsett, L.; El Khoury, J. Microglia in Neurodegeneration. *Nat. Neurosci.* **2018**, *21* (10), 1359–1369.

(53) Venegas, C.; Heneka, M. T. Danger-Associated Molecular Patterns in Alzheimer's Disease. *J. ofLeukocyte Biol.* **2017**, *101* (1), 87–98.

(54) Yang, L.; Liu, C. C.; Zheng, H.; Kanekiyo, T.; Atagi, Y.; Jia, L.; Wang, D.; N'songo, A.; Can, D.; Xu, H.; et al. LRP1 Modulates the Microglial Immune Response via Regulation of JNK and NF-KB Signaling Pathways. *J. Neuroinflammation* **2016**, *13* (1), 1–13.

(55) O'Brien, C. E.; Wyss-Coray, T. Sorting through the Roles of Beclin 1 in Microglia and Neurodegeneration. *J. Neuroimmune Pharmacol.* **2014**, *9* (3), 285–292.

(56) Roodveldt, C.; Labrador-Garrido, A.; Gonzalez-Rey, E.; Lachaud, C. C.; Guilliams, T.; Fernandez-Montesinos, R.; Benitez-Rondan, A.; Robledo, G.; Hmadcha, A.; Delgado, M.; et al. Preconditioning of Microglia by α-Synuclein Strongly Affects the Response Induced by Toll-like Receptor (TLR) Stimulation. *PLoS One* **2013**, *8* (11), 1–17.

(57) McDonald, C. L.; Hennessy, E.; Rubio-Araiz, A.; Keogh, B.; McCormack, W.; McGuirk, P.; Reilly, M.; Lynch, M. A. Inhibiting TLR2 Activation Attenuates Amyloid Accumulation and Glial Activation in a Mouse Model of Alzheimer's Disease. *Brain. Behav. Immun.* **2016**, *58*, 191–200.

(58) Zhu, Y.; Hou, H.; Rezai-Zadeh, K.; Giunta, B.; Ruscin, A.; Gemma, C.; Jin, J.; Dragicevic, N.; Bradshaw, P.; Rasool, S.; et al. CD45 Deficiency Drives Amyloid- Peptide Oligomers and Neuronal Loss in Alzheimer's Disease Mice. *J. Neurosci.* **2011**, *31* (4), 1355–1365.

(59) Labrador-Garrido, A.; Cejudo-Guillén, M.; Daturpalli, S.; Leal, M. M.; Klippstein, R.; De Genst, E. J.; Villadiego, J.; Toledo-Aral, J. J.; Dobson, C. M.; Jackson, S. E.; et al. Chaperome Screening Leads to Identification of Grp94/Gp96 and FKBP4/52 as Modulators of the a-Synuclein-Elicited Immune Response. *FASEB J.* **2016**, *30* (2), 564–577.

(60) Cox, J.; Mann, M. MaxQuant Enables High Peptide Identification Rates, Individualized p.p.b.-Range Mass Accuracies and Proteome-Wide Protein Quantification. *Nat. Biotechnol.* **2008**, *26* (12), 1367–1372.

(61) Cox, J.; Hein, M. Y.; Luber, C. A.; Paron, I.; Nagaraj, N.; Mann, M. Accurate Proteome-Wide Label-Free Quantification by Delayed Normalization and Maximal Peptide Ratio Extraction, Termed MaxLFQ. *Mol. Cell. Proteomics* **2014**, *13* (9), 2513–2526.

high
IL-1β
IL-6
TNFα

Type B
oligomers

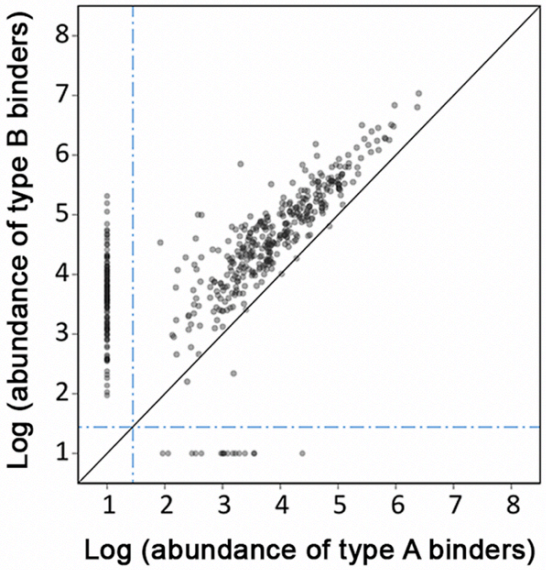

Type A
oligomers

low
IL-1β
IL-6
TNFα

Supplementary information

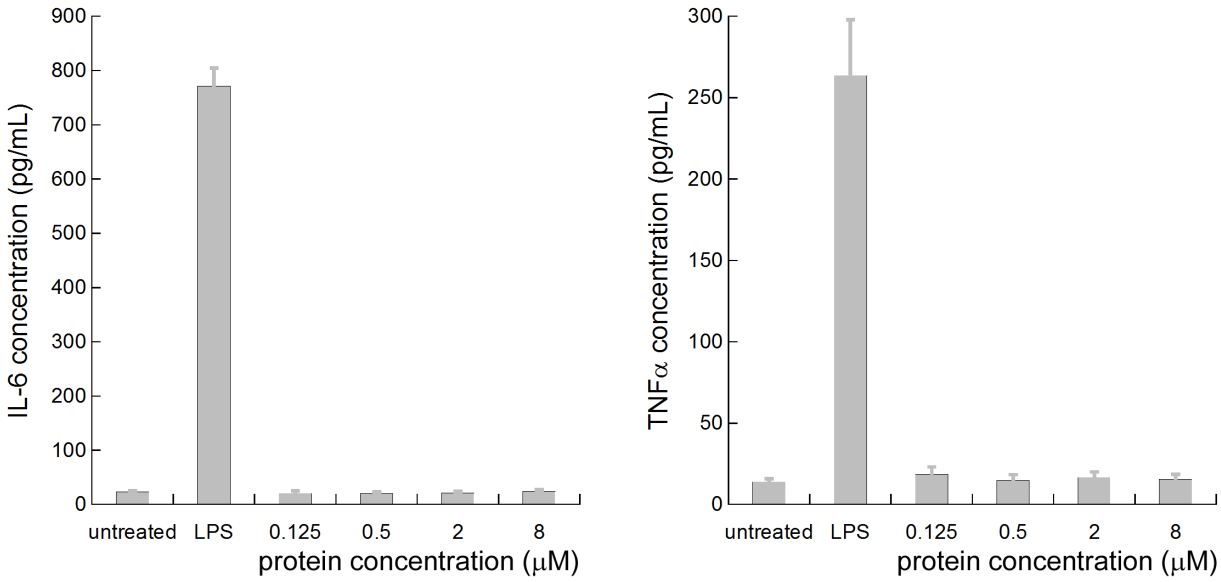

Supplementary Figure 1. Cytokine release profile of N13 microglia cells after treatment with monomeric HypF-N. The release of IL-6, and TNFα was measured by ELISA assays in the supernatants of cultured N13 cells treated with 0.125 μM, 0.25 μM, 2 μM and 8 μM concentrations of native non-aggregated HypF-N. The culture medium with and without addition of LPS was used as a negative and positive control, respectively. The error bars correspond to standard errors of the mean (SEM) with n=4. The treatment with native non-aggregated HypF-N results in secretion of these cytokines at levels indistinguishable from untreated cells.

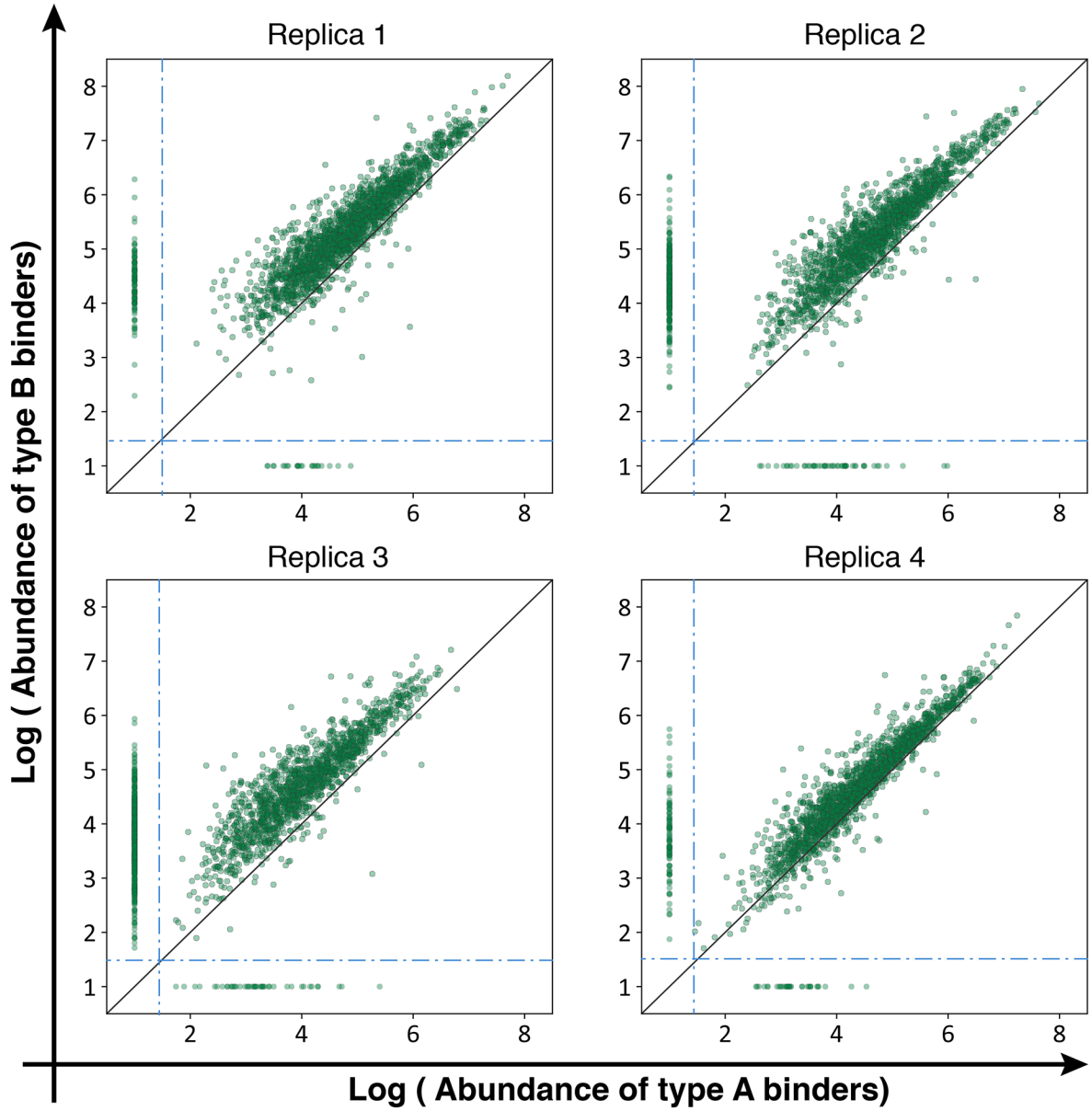

Supplementary Figure 2. Interactions of type A and type B oligomers with the cytosolic proteins from N13 cells. Replica-specific scatterplot of protein abundances (log_{10} iBAQ values) of N13 microglia cell proteins bound to type B oligomers (y axis) *vs* those bound to type A oligomers (x axis) in the four biological replicas analysed. The green points in each subplot represent cytosolic proteins detected and quantified in each replica. Proteins shown vertically on the left and horizontally on the lower edge of each scatterplot are proteins binding only to type B and type A oligomers, respectively.